Biosensors and Bioelectronics 57 (2014) 48–53

Contents lists available at ScienceDirect

Biosensors and Bioelectronics

journal homepage: www.elsevier.com/locate/bios

Wheatstone bridge giant-magnetoresistance based cell counter

Chiun-Peng Lee [a,1], Mei-Feng Lai [b,1], Hao-Ting Huang [a], Chi-Wen Lin [b], Zung-Hang Wei [a,*]

[a] Department of Power Mechanical Engineering, National Tsing Hua University, Taiwan ROC
[b] Institute of Nanoengineering and Microsystems, National Tsing Hua University, No. 101, Section 2, Kuang-Fu Road, Hsinchu 30013, Taiwan ROC

ARTICLE INFO

Article history:
Received 28 October 2013
Received in revised form
6 January 2014
Accepted 17 January 2014
Available online 25 January 2014

Keywords:
Giant magnetoresistance
Biosensor
Cell counting
Cell separation

ABSTRACT

A Wheatstone bridge giant magnetoresistance (GMR) biosensor was proposed here for the detection and counting of magnetic cells. The biosensor was made of a top-pinned spin-valve layer structure, and it was integrated with a microchannel possessing the function of hydrodynamic focusing that allowed the cells to flow in series one by one and ensured the accuracy of detection. Through measuring the magnetoresistance variation caused by the stray field of the magnetic cells that flowed through the microchannel above the GMR biosensor, we can not only detect and count the cells but we can also recognize cells with different magnetic moments. In addition, a magnetic field gradient was applied for the separation of different cells into different channels.

1. Introduction

Magnetism provides great opportunities for researchers to remotely control and detect small biological samples for biomicrofluidic applications. Since last decade, there has been some research on magnetic biochips (Pamme, 2006) such as magnetic micromixing (Rida and Gijs, 2004; Roy et al., 2009; Wei and Lee, 2009), sample separation (Rong et al., 2006; Drogoff et al., 2008; Lee and Lai, 2010), and magnetic manipulation of biological samples (Vieira et al., 2009; Lai et al., 2010; Lee et al., 2012). Besides, quantitative detection of biological samples using magnetic approaches is also an important topic of research.

Magnetic immunoassay is one novel type of immunoassays that can quantitatively detect biomolecules. The mechanism of magnetic immunoassay is that magnetic labels/beads are conjugated to either an antibody or an antigen that is specifically binding to the antibody. The quantity of the analyte is proportional to the magnetic beads, whose quantity can be determined by a magnetic measurement, such as measuring the remanent magnetic flux (Enpuku et al., 1999) or the magnetization relaxation time (Matz et al., 2001) of magnetic particle clusters, measuring the reduction of AC magnetic susceptibility of the mixture (Krause et al., 2007; Nikitin et al., 2007), and using an optical approach to measure the amount of two-particle structures created by the conjugation between antigens and antibodies (Ranzoni et al., 2011).

In addition to the methods mentioned above, magnetoresistance (MR) can also be used for determining the quantity of the analyte in magnetic biosensing. The amount of target biomolecules/cells can be estimated by measuring the MR signal variation of the MR-based biosensor caused by the magnetic micro- or nanoparticles that are attached on the target sample. In 2008 Osterfeld et al. proposed a prototypical MR-based biosensor (Osterfeld et al., 2008) that can detect the target molecules attached with magnetic nanoparticles through MR measurement. Similarly, Vavassori et al. utilized magnetic domain walls of patterned ferromagnetic films to attract nanomeric magnetic beads, and estimated the amount of beads according to the MR variation of the ferromagnetic films (Vavassori et al., 2008). So far, cell detection using MR-based biosensors is seldom referred to in the literature partly because it is more challenging than biomolecule detection (Huang et al., 2013). In this study, we designed an MR-based biosensor that can be used to count flowing magnetically-labeled cells in a microfluidic channel. In addition, the sorting of different cells was also demonstrated in our experiment.

Flow cytometer, which can rapidly count and separate cells that belong to different populations, is one of the most important instruments in the field of basic and clinical medicine (Vignali, 2000), and it has been widely used for the research on cell immunoassay, cell cycle, ploidy analysis (Tzur et al., 2011), and so on. Today, most of the flow cytometers are based on the fluorescent sensing technology. This technology is mature and practical, but the cost is very high. Therefore, the purpose of this study is to develop an alternative technique that is more economical for cell counting by the integration of the highly-developed spintronics and microfluidics.

2. Experiment details

2.1. Cell counter design

Fig. 1 shows the schematic of the magnetic cell counter setup. The cell counter was composed of a giant-magnetoresistance (GMR)

* Corresponding author. Tel.: +88 6 3 5715131x33603; fax: +88 6 3 5722840.
E-mail address: wei@pme.nthu.edu.tw (Z.-H. Wei).
[1] These authors contributed equally to this work.

0956-5663/$ - see front matter © 2014 Elsevier B.V. All rights reserved.
http://dx.doi.org/10.1016/j.bios.2014.01.028

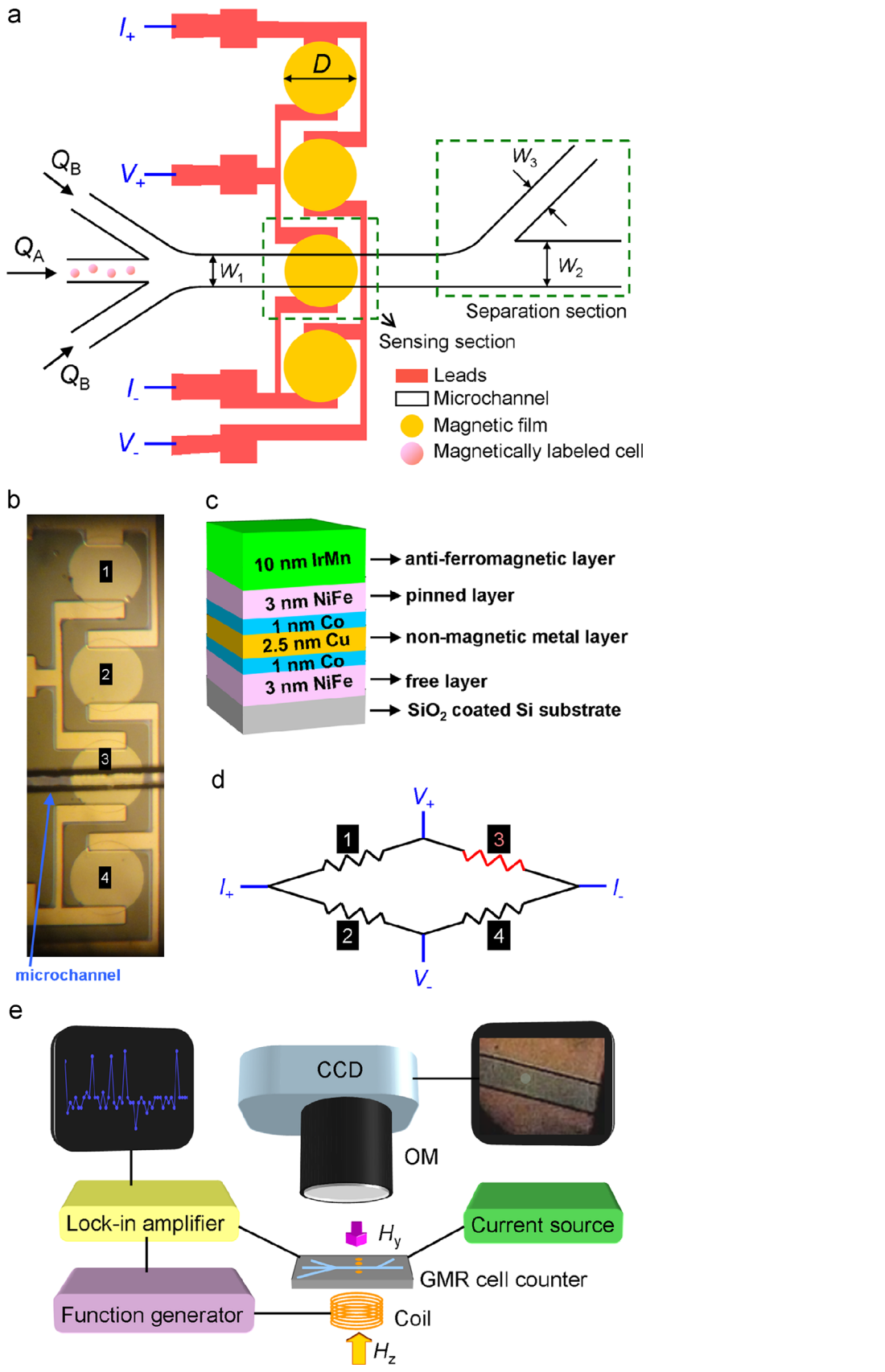

Fig. 1. (a) Schematic of the spin-valve GMR cell counter structure. (b) Micrograph of the Wheatstone bridge composed of four GMR discs, the third of which is traversed by the microchannel. (c) The layer structure of the spin valve used in this study. (d) Equivalent circuit of the Wheatstone bridge in (a) and (b), in which I_+, I_-, V_+ and V_- indicate the current and voltage connecting points for the electrical measurements. (e) Experimental setup for the cell detection. (For interpretation of the references to color in this figure, the reader is referred to the web version of this article.)

sensor and a microchannel that included an upstream section for the hydrodynamic focusing of cell solution, a sensing section for cell detection [see the sensing section in Fig. 1(a)], and a downstream section for cell separation [see the separation section in Fig. 1(a)]. At the head of the upstream section there were three inlets, the central of which was for the inflow (with flow rate Q_A) of the cell solution, and the two symmetric side channels were for the buffer inflow (each with flow rate Q_B). Through hydrodynamic focusing we can focus the flow width of the cell solution to be about of the cell size such that cells can flow in series rather than side by side when passing through the sensing section to ensure the accuracy of cell counting. The sensing section of the microchannel with a GMR sensor underneath was 250 μm long, 60 μm wide [see the W_1 in Fig. 1(a)], and 47 μm high. The separation section was designed for the separation of cells that have different magnetic moments. Cells with larger magnetic moment can be guided into the branch channel by means of applying a magnetic field gradient.

In recent years, GMR biosensors have been used to measure magnetically-labeled biomolecules/cells (Srinivasan et al., 2011; Shoshi et al., 2012; Loureiro et al., 2011). Srinivasan et al. proposed a GMR biosensor that can estimate the amount of magnetically-labeled endoglin (Srinivasan et al., 2011). Shoshi et al. proposed a GMR sensor that was designed for detecting the amount of magnetic particles entering a living cell that was fixed on the GMR sensor (Shoshi et al., 2012). Loureiro et al. proposed a GMR spin-valve biosensor for magnetic cell detection, and the amount of cells was estimated using a filtering technique (Loureiro et al., 2011).

Our biosensor was made of a Wheatstone bridge [see Fig. 1 (b) for the optical microscope (OM) image] that consisted of four circular GMR discs made of the same size and material. The usage of the Wheatstone bridge not only can enhance the sensing sensitivity, but also can prevent the measurement from being influenced by the noise and signal shift caused by environmental perturbations such as thermal disturbance (Wang et al., 2005). The magnetic discs, each with a diameter of 250 μm, were top-pinned spin valves with the layer structure of IrMn(10 nm)/NiFe(3 nm)/Co (1 nm)/Cu(2.5 nm)/Co(1 nm)/NiFe(3 nm) [see Fig. 1(c)], where the top IrMn layer was an anti-ferromagnetic layer, and the Co layer was the immiscible layer. The principle of cell detection by the Wheatstone bridge GMR biosensor is as follows: when a magnetically-labeled cell passes through the channel above the GMR disc, a stray field from the cell affects the electrical resistance of the disc, and the electrical resistance variation is dependent on the magnitude of the stray field. Meanwhile, by measuring the number and magnitude of the peaks in the resistance vs. time curve, we can estimate the number and the relative magnetic moments of the cells. Fig. 1(d) shows the equivalent circuit of the Wheatstone bridge GMR biosensor. The sensing section of the microchannel was located above the GMR disc number 3 [also see Fig. 1(a) and (b)], so an electric potential difference between V_+ and V_- occurred when the stray field from the flowing cells affected the resistance of disc number 3.

The fabrication process of the GMR cell counter consisted of three main steps: fabrication of the GMR sensor, fabrication of the microchannel, and the integration of the above. Some details of the fabrication process are introduced in the Supplementary document (see Fig. S1 in the supplementary document). After the fabrication of the spin valve, Au electrodes were deposited on the spin valve for electrical signal measurement. The microchannel was made of PDMS, and was fabricated via a SU-8 photoresist molding method.

Fig. 1(e) shows the experiment setup for measuring the electrical potential variation of the GMR sensor. In the in-plane direction of the GMR discs, we applied a bias-field H_y with a magnitude large enough to make the GMR spin valve most sensitive to the external field. The way to determine the optimum H_y will be discussed later. Besides, we also put a coil under the cell counter to provide an out-of-plane alternating magnetic field H_z [223 Hz with a field strength of 29 ± 1.3 Gauss, see the yellow arrow in Fig. 1(e)]. The function of the AC coil was to magnetize the cells such that the stray field of the cells can alternate at a fixed frequency, and we can record the influence of the cells on the resistance of the GMR sensor by a phase locking technique. For the electrical potential measurement of the Wheatstone bridge, we used a current source (6221 current source, Keithley) to provide a constant current of 1 mA, and used a lock-in amplifier (SR830, Stanford Research Systems) with sampling rate 512 Hz to measure the potential variation. The driving source of the AC coil was a function generator (SFG830, GW INSTEK), which also provided the lock-in amplifier with the reference frequency. To make sure whether the electrical potential variations were caused by the magnetically-labeled cells, we took videos of the cells by using a microscope equipped with CCD when they were passing through the GMR sensor area.

2.2. MR measurement

Fig. 2 shows the MR curve of a single GMR disc obtained from a four-point measurement that can be used to determine the above-mentioned optimum H_y magnitude for highest sensitivity of the sensor. The inset of Fig. 2 shows the schematic of the experimental setup for the MR curve measurement, in which the black arrow indicates the direction of the positive magnetic field. The definition of the MR ratio in y-axis label is $[(R-R_{min})/R_{min}]\times 100\%$ (Wegrowe et al., 1999), where R_{min} is the lowest resistance, and R is the resistance at an arbitrary field. As shown in Fig. 2, when the external field was in the range of 35–65 Gauss the steepest MR ratio with respect to field change occurred, so we chose H_y to be 50 Gauss, which was the average of 35 and 65 Gauss.

2.3. Cell preparation

The cells used in this study were mouse monocyte-macrophage cells (RAW 264.7) and nasopharyngeal carcinoma cells (NPC-TW01), which are both adhesive cells. They were cultured in a Dulbecco's modified Eagle's medium (DMEM, Hyclone) containing 10% fetal bovine serum (FBS, Millipore), 4 mM L-glutamine, 4500 mg/L glucose, and 1% penicillin (Biological Industries) at 37 °C and 5% CO_2 environment. To make the cells magnetically labeled, they were co-cultured with a diluted (1 μg/mL) water-based ferrofluid (EMG705, Ferrotec) containing 10 nm Fe_3O_4

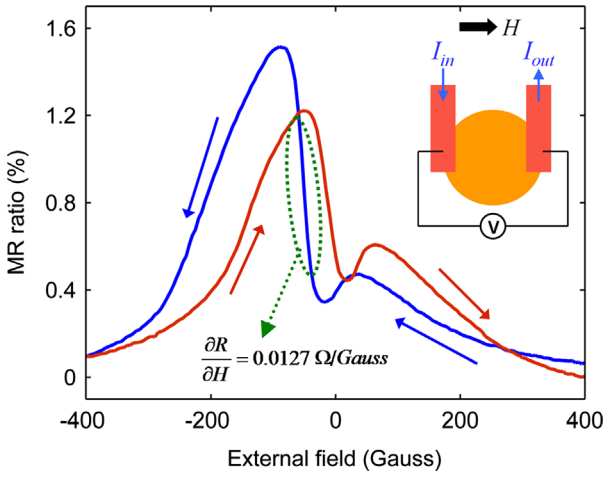

Fig. 2. MR curve of a single GMR disc. The inset is the schematic of the four-point resistance measurement under magnetic field H.

magnetic nanoparticles (3.9% in volumetric concentration) for 24 h. The magnetic nanoparticles then entered the cells by endocytosis, and the cells that contained magnetic nanoparticles were collected by a permanent magnet and purified by centrifugation. The cells were then put in a clean culture solution.

To verify that the cells can keep alive during ferrofluid co-culture, cell viability was examined through a dye exclusion test. The cells were stained by 0.4% Trypan blue (Invitrogen) that was mixed with RPMI media (Gibco) in 1:1 volume ratio. The dye only infiltrated the dead cells and stained them blue, whereas the living cells were left unstained, and therefore the cell viability can be obtained. We used a hemocytometer to count the number α of the living cells and β of the dead cells under an OM, and calculated the cell viability $\alpha/(\alpha+\beta)$ as shown in Fig. S2(a) and (b) (see the Supplementary document) for RAW and NPC cells, respectively. From Fig. S2 we observed that the cell viabilities for both RAW and NPC cells were close to 90% after 12 h of co-culture with ferrofluid. Even after 24 h of co-culture, it showed no significant difference between the experimental group and the negative control group, where ferrofluid was absent during culturing. The high cell viability proves that the ferrofluid co-culture basically did no harm to the cells.

3. Results and discussion

3.1. Cell counting

Before we measured the response of the biosensor from different types of cells, we tested the effect of hydrodynamic focusing on the acquired electrical signals. Fig. 3(a) and (b) shows the electrical signals of the Wheatstone bridge GMR biosensor for RAW cells without and with hydrodynamic focusing, respectively. The magnitude of the voltage peaks in the figures reflected the variation of resistance in GMR disc no. 3 (see Fig. 1) caused by the stray field of the cells when the cells flowed through. In comparison, the peaks in Fig. 3(a) without hydrodynamic focusing were random in contrast to the peaks in Fig. 3(b) with hydrodynamic focusing. The standard deviation of the peaks was ± 0.18 μV in Fig. 3(a) and ± 0.09 μV in Fig. 3(b). It means that by restricting the transverse range of cell flow using hydrodynamic focusing, we can effectively acquire more uniform signals for analysis, where narrow band-pass filtering can be used to accurately estimate the cell number.

Fig. 3(c) shows the electrical signal of the biosensor for NPC cells with hydrodynamic focusing. Based on ten measurements, we obtained that the average peaks were 0.42 ± 0.09 μV for RAW cells in Fig. 3(b) and 0.91 ± 0.14 μV for NPC cells in Fig. 3(c), so the signal-to-noise ratio was about 2.2 times larger in Fig. 3(c) than that in Fig. 3(b), which is believed to be caused by the different numbers of magnetic nanoparticles inside an RAW cell and an NPC cell. To clarify this, magnetophoresis experiment was performed here to estimate the numbers of magnetic nanoparticles inside a cell. In this experiment, the cells moved at a constant speed when the viscous force and the magnetic force balanced out, which can be expressed as $6\pi\eta r v = NbM_s(\pi d^3/6)\nabla B$ (Wilhelm et al., 2002), where η is the viscosity of the cell medium (1.15×10^{-3} Pa s for DMEM), r is the radius of a cell, v is the cell velocity, N is the number of magnetic nanoparticles within a cell, $b=0.8$ is the ratio of the net magnetization of magnetic nanoparticles to their saturation magnetization M_s (Kalambur et al., 2007), d is the diameter of the magnetic nanoparticle, and ∇B is the magnetic field gradient exerted on a cell, which was 16 mT/mm in the present case. The average cell radius and cell velocity for RAW cells were 6 μm and 2.85 μm/s, respectively, and those for NPC cells were 9 μm and 4.66 μm/s, respectively. From the above equation,

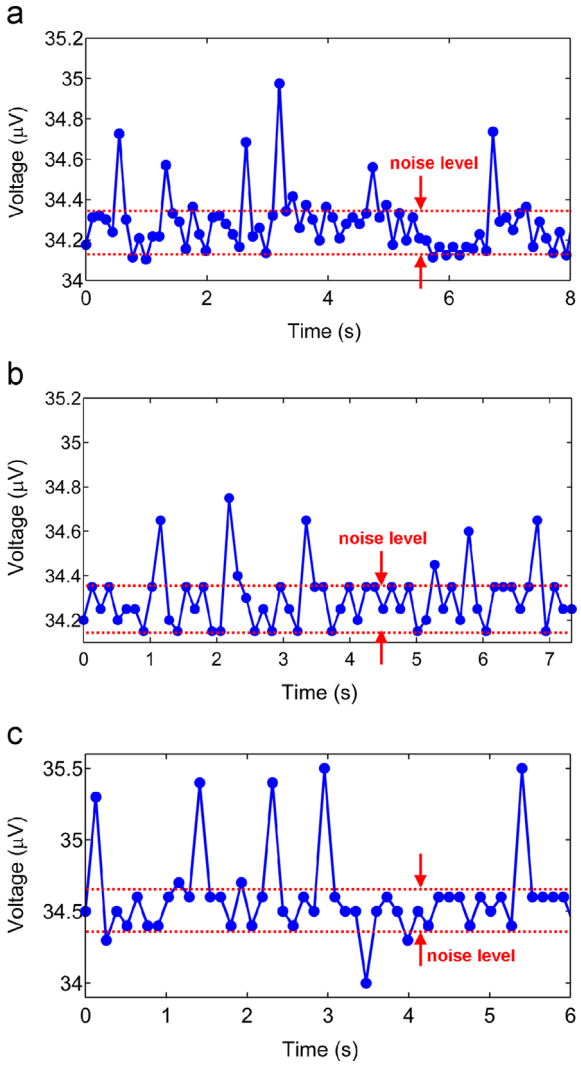

Fig. 3. Detection results of (a) RAW cells being pumped into the microchannel without hydrodynamic focusing, (b) RAW cells with hydrodynamic focusing, and (c) NPC cells with hydrodynamic focusing. The flow rates Q_A and Q_B for the focusing were 0.2 μL/min and 0.1 μL/min, respectively. The focus width of the cell solution was about 20 μm.

the magnetic nanoparticles inside each cell can be estimated to be 3.14×10^6 for an RAW cell and 7.71×10^6 for an NPC cell, which was 2.45 times more than an RAW cell. This can explain why the measured voltage peaks for NPC cells were about 2.2 times larger than those for RAW cells as mentioned above, and it indicates that our designed GMR cell counter has the ability to recognize cells with different numbers of magnetic nanoparticles. The correspondence between the measured peaks in Fig. 3(c) and the dynamics of the cell flow was given in Supplementary movie 1, along with a supplementary document for a brief introduction. From comparison we observed that each voltage peak corresponded to the very moment when a cell flowed through the channel above the biosensor.

Supplementary material related to this article can be found online at http://dx.doi.org/10.1016/j.bios.2014.01.028.

To further demonstrate the cell recognition ability of our designed cell counter, we injected a mixture solution of RAW cells and NPC cells into the microchannel. Fig. 4 shows the electrical signals obtained in two independent measurements. The correspondence between the measured peaks in Fig. 4(a) and (b) and the dynamics of the cell flow was also given in Supplementary movies 2 and 3, respectively. From Fig. 4 we observed that when two different types of magnetic cells existed in the microchannel,

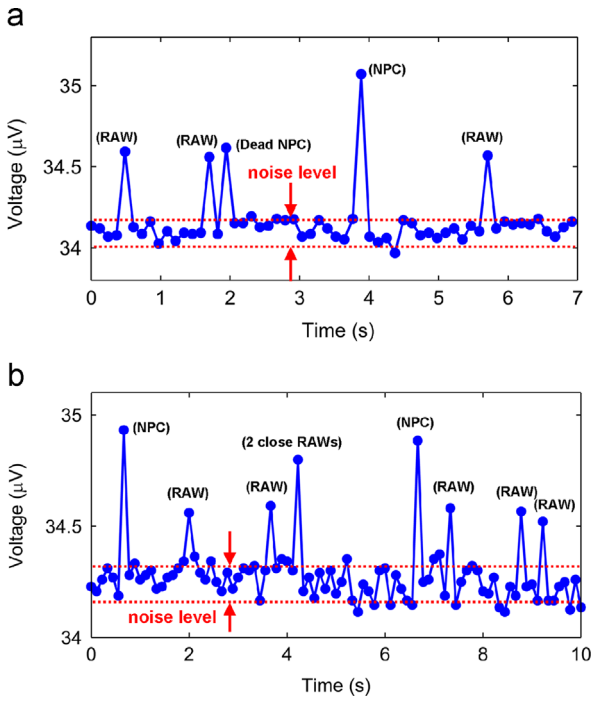

Fig. 4. Results of the cell detection when RAW cells and NPC cells were pumped into the microchannel simultaneously. (a) and (b) Detection results obtained in two independent measurements. The flow rates Q_A and Q_B were 0.2 μL/min and 0.1 μL/min, respectively. The focus width of the cell solution was about 20 μm.

the designed cell counter can clearly recognize them; besides, the measured peaks for RAW cells and NPC cells exhibited a ratio similar to the one found in Fig. 3(b) and (c). From the results shown in Figs. 3 and 4 we can see that the combination of the Wheatstone bridge GMR biosensor and the lock-in technique can not only prevent the measurement from being influenced by the environmental perturbations, but also enhance the signal-to-noise ratio to up to 4 without using any filter. Therefore, we could easily recognize cells that engulfed different numbers of magnetic nanoparticles. To further examine the advantage of using the Wheatstone bridge GMR discs configuration over using a single GMR disc configuration, we compared the background noise signals that were recorded using these two configurations (see Fig. S3 in the supplementary document). For the Wheatstone bridge configuration, the average amplitude of the noise was 3.2 times smaller than the one for single GMR disc. This comparison reveals that the usage of the Wheatstone bridge can effectively reduce the average noise amplitude.

3.2. Cell separation

In addition to cell detection, our designed cell counter also has the function of cell sorting for the cells with different magnetic moments. The mechanism for cell sorting is that the magnetic field gradient is applied to cause a deflection of the cell motion, and the cells with larger magnetic moment are easier to be attracted to the branch channel along the direction of the magnetic field gradient [see the cell and the dashed red arrow in Fig. 5(a)]. The green pillar

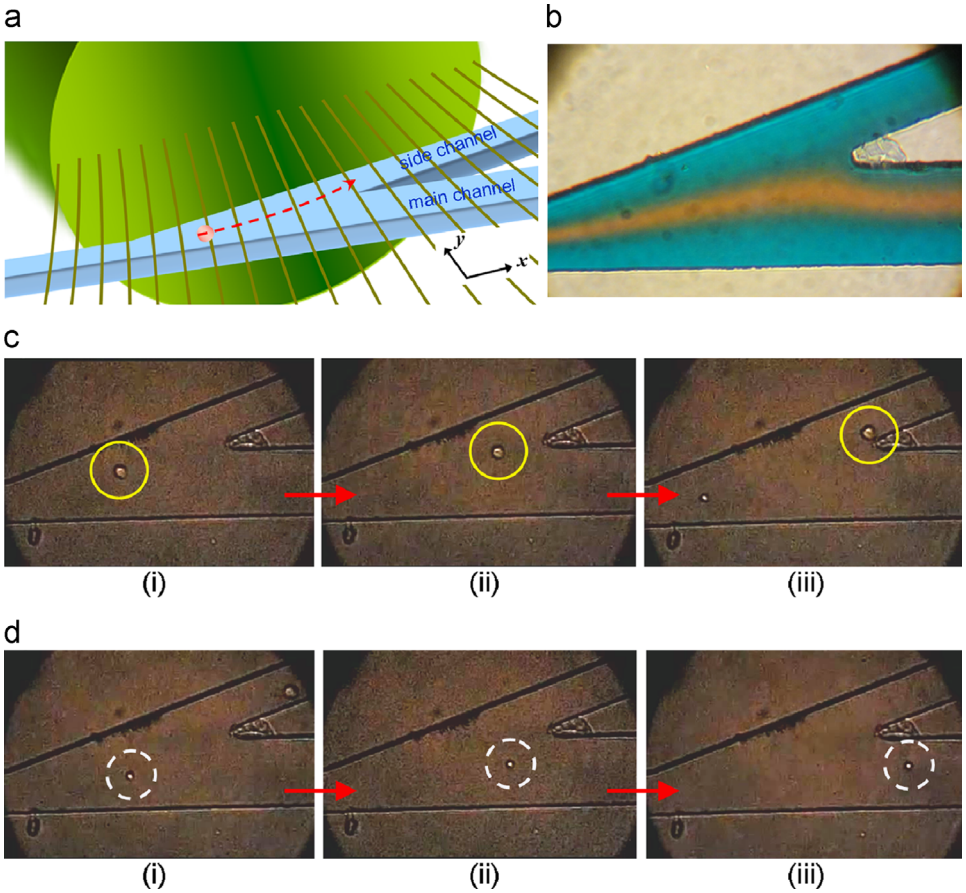

Fig. 5. (a) Schematic of cell separation under a magnetic field gradient. The green (solid) lines indicate the magnetic field lines. (b) Dyed water flow (in orange) that simulated the flowing direction of the cell solution stream (the central stream) with hydrodynamic focusing. The ratio of Q_A to Q_B was 2. (c) and (d) Sequential micrographs for the magnetic cell separation of (c) an NPC cell (marked by the solid yellow circles) and (d) a RAW cell (marked by the dashed white circles). (For interpretation of the references to color in this figure legend, the reader is referred to the web version of this article.)

Table 1
Required magnetic field gradient for separating RAW and NPC cells vs. fluid flow rates Q_A and Q_B

Q_A (μL/min)	Q_B (μL/min)	∇B(mT/mm)
0.2	0.1	8
0.4	0.2	18
0.6	0.3	26

in Fig. 5(a) represents one end of a permanent magnet that was used for producing a magnetic field gradient, and the blue area represents the separation section of the microchannel in this research. The green curves represent the magnetic field lines produced by the magnet. The width of the main channel was designed to expand from 60 μm to 100 μm [see the W_1 and W_2 in Fig. 1(a)] in the intersection of the separation section such that the central flow could approach the branch channel [demonstrated in the test experiment shown in Fig. 5(b)], and therefore a small magnetic field gradient was enough to make the magnetic cells flow into the branch channel.

Fig. 5(c) and (d) represents the sequential micrographs for the magnetic cell separation of an NPC cell [see Fig. 5(c)] and an RAW cell [see Fig. 5(d)] (see Supplementary movie 4 for the dynamics of cell separation). The flow rates were Q_A= 0.2 μL/min for the central channel and Q_B=0.1 μL/min for the two side channels, and the magnetic field gradient was 8 mT/mm. From Fig. 5(c) and (d) we observed that the NPC cell, which on average carried 2.45 times more magnetic nanoparticles than an RAW cell, diverted to the branch channel and the RAW cell remained in the main channel. Table 1 shows the magnetic field gradient required to separate NPC cells and RAW cells for different values of Q_A and Q_B, and it can be observed that the magnetic field gradient required was linearly proportional to Q_A and/or Q_B.

4. Conclusions

In summary, we proposed a Wheatstone bridge GMR biosensor for magnetic cell detection. Using the designed biosensor, we not only can detect cells but we can also sort cells with different magnetic moments as well, which was verified by comparing the measured electrical signals of the biosensor and the number of magnetic nanoparticles obtained from the magnetophoresis experiment. In addition, we also used a magnetic field gradient for the separation of different cells into different channels. The experimental result shows that the designed magnetic cell counter can serve as an alternative of the optical cell counters. Our research results will have a great impact on future development and applications of biosensors.

Acknowledgment

This work was supported partly by the ROC National Science Council Grant numbers NSC 99-2112-M-007-016-MY3, NSC 99-2112-M-007-015-MY3, NSC 102-2112-M-007-006-MY3 and NSC 102-2112-M-007-012-MY3.

Appendix A. Supplementary material

Supplementary data associated with this article can be found in the online version at http://dx.doi.org/10.1016/j.bios.2014.01.028.

References

Drogoff, B.L., Clime, L., Veres, T., 2008. Microfluid. Nanofluid. 5, 373–381.
Enpuku, K., Minotani, T., Gima, T., Kuroki, Y., Itoh, Y., Yamashita, M., Katakura, Y., Kuhara, S., 1999. Jpn. J. Appl. Phys. 38, 1102–1105.
Huang, H.T., Ger, T.R., Lin, Y.H., Wei, Z.H., 2013. Lab Chip 13, 3098–3104.
Kalambur, V.S., Longmire, E.K., Bischof, J.C., 2007. Langmuir 23, 12329–12336.
Krause, H.J., Wolters, N., Zhang, Y., Offenhäusser, A., Miethe, P., Meyer, M.H.F., Hartmann, M., Keusgen, M., 2007. J. Magn. Magn. Mater. 311, 436–444.
Lai, M.F., Chen, C.Y., Lee, C.P., Huang, H.T., Ger, T.R., Wei, Z.H., 2010. Appl. Phys. Lett. 96, 183701.
Lee, C.P., Lai, M.F., 2010. J. Appl. Phys. 10709B524.
Lee, C.P., Tsai, H.Y., Lai, M.F., 2012. Appl. Phys. Lett. 100, 264102.
Loureiro, J., Andrade, P.Z., Cardoso, S., da Silva, C.L., Cabral, J.M., Freitas, P.P., 2011. Lab Chip 11, 2255–2261.
Matz, H., Hartwig, S., Kerberger, T., Atzpadin, H., Trahms, L., 2001. IEEE Trans. Magn. 11, 1371–1374.
Nikitin, P.I., Vetoshko, P.M., Ksenevich, T.I., 2007. J. Magn. Magn. Mater. 311, 445–449.
Osterfeld, S.J., Yu, H., Gaster, R.S., Caramuta, S., Xu, L., Han, S.J., Hall, D.A., Wilson, R. J., Sun, S., White, R.L., Davis, R.W., Pourmand, N., Wang, S.X., 2008. Proc. Natl. Acad. Sci. USA 105, 20637–20640.
Pamme, N., 2006. Lab Chip 6, 24–38.
Ranzoni, A., Schleipen, J.J.H.B., van IJzendoorn, L.J., Prins, M.W.J., 2011. Nano Lett. 11, 2017–2022.
Rida, A., Gijs, M.A.M., 2004. Anal. Chem. 76, 6239–6246.
Rong, R., Choi, J.W., Ahn, C.H., 2006. J. Micromech. Microeng. 16, 2783–2790.
Roy, T., Sinha, A., Chakraborty, S., Ganguly, R., Puri, I.K., 2009. Phys. Fluids 21, 027101.
Shoshi, A., Schotter, J., Schroeder, P., Milnera, M., Ertl, P., Charwat, V., Purtscher, M., Heer, R., Eggeling, M., Reiss, G., Brueckl, H., 2012. Biosens. Bioelectron. 36, 116–122.
Srinivasan, B., Li, Y., Jing, Y., Xing, C., Slaton, J., Wang, J.P., 2011. Anal. Chem. 83, 2996–3002.
Tzur, A., Moore, J.K., Jorgensen, P., Shapiro, H.M., Kirschner, M.W., 2011. PLoS One 6, e16053.
Vavassori, P., Metlushko, V., Ilic, B., Gobbi, M., Donolato, M., Cantoni, M., Bertacco, R., 2008. Appl. Phys. Lett. 93, 203502.
Vieira, G., Henighan, T., Chen, A., Hauser, A.J., Yang, F.Y., Chalmers, J.J., Sooryakumar, R., 2009. Phys. Rev. Lett. 103, 128101.
Vignali, D.A.A., 2000. J. Immunol. Methods 243, 243–255.
Wang, D., Brown, J., Hazelton, T., Daughton, J., 2005. IEEE Trans. Magn. 42, 3700–3702.
Wegrowe, J.E., Kelly, D., Franck, A., Gilbert, S.E., Ansermet, J.P., 1999. Phys. Rev. Lett. 82, 3681–3684.
Wei, Z.H., Lee, C.P., 2009. J. Appl. Phys. 10507B523
Wilhelm, C., Gazeau, F., Bacri, J.C., 2002. Eur. Biophys. J. 31, 118–125.